Small-Signal Analysis of DCM Flyback Converter in Frequency-Foldback Mode of Operation

Laszlo Huber and Milan M. Jovanović
Delta Products Corporation
P.O. Box 12173
5101 Davis Drive
Research Triangle Park, NC 27709, USA

Abstract - **The predicted closed-loop bandwidth of the DCM flyback converter in frequency-foldback mode (FFM) of operation obtained by the conventional averaged small-signal model that models the voltage-controlled oscillator (VCO) with a constant gain does not change with the load. However, this prediction is not in agreement with the closed-loop measurements. In this paper, the discrepancy between the conventional averaged small-signal model and measurements is systematically investigated. It is found that the source of this discrepancy is the nonlinearity of the VCO that generates sideband frequency components and, therefore, cannot be modeled as a constant-gain transfer function. By including the effect of the sideband components in the closed loop, a multi-frequency averaged small-signal model of the DCM flyback converter in the FFM which accurately predicts the loop bandwidth behavior with the load is proposed.**

I. INTRODUCTION

The flyback converter is a popular topology for low-power applications such as, for example, notebook adapters/chargers, because of its simplicity and cost effectiveness. A typical operation profile of the flyback adapters/chargers is shown in Fig. 1. At heavy loads, they operate at the boundary of the discontinuous conduction mode (DCM) and continuous conduction mode (CCM), also called quasi-resonant mode (QRM), with valley switching (VSW) of the flyback switch. As shown in Fig. 1, in QRM the switching frequency increases as the load decreases. To prevent high-frequency operation at lighter loads, the quasi-resonant operation changes to DCM operation with valley switching, where the switching frequency is approximately constant and equal to its maximum value. To meet the challenging high-efficiency requirements in the entire load range [1], [2], at light loads the operation changes from DCM with constant switching frequency and valley switching to DCM with variable switching frequency, where the switching frequency linearly decreases as the load decreases. This mode of operation is known as frequency-foldback mode (FFM). The FFM can be implemented with or without valley switching.
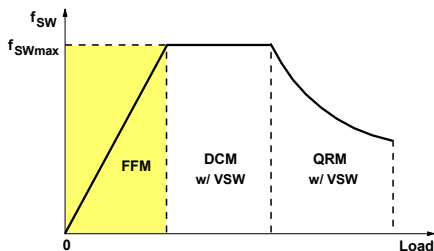

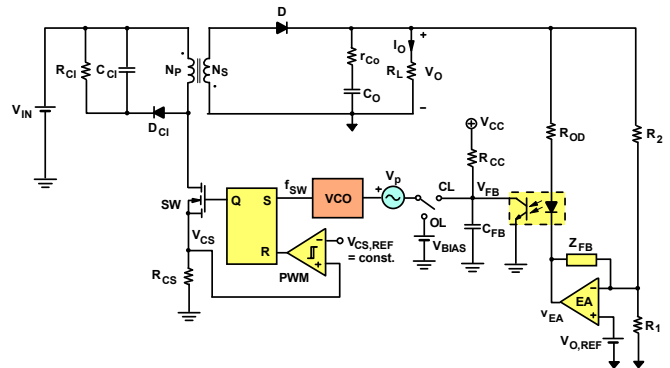Fig. 1 Typical operation profile of flyback adapters/chargers

Fig. 2 Simplified circuit diagram of DCM flyback converter in FFM (V_p - perturbation voltage source, CL - closed loop, OL - open loop)

The simplified circuit diagram of the DCM flyback converter operating in the FFM is presented in Fig. 2. The switching frequency f_{sw} is controlled by the feedback voltage V_{FB} using a voltage-controlled oscillator (VCO). The circuit diagram of the VCO is shown in Fig. 3(a); whereas, the transfer function of the VCO is shown in Fig. 3(b). As the load decreases, the feedback voltage decreases and, consequently, the switching frequency decreases. The main switch turns on by the VCO and turns off when the current-sense (CS) voltage V_{CS} reaches reference voltage level $V_{CS,REF}$. If the peak value of the sensed current pulses is constant, the switching frequency linearly varies with the load current. It should be noted that voltage source V_p shown in Fig. 2 is the perturbation voltage source, which was only used in simulations aimed to study the open- and closed-loop behavior of the converter. It does not exist in the hardware, i.e., in a real circuit node CL is directly connected to the VCO input.
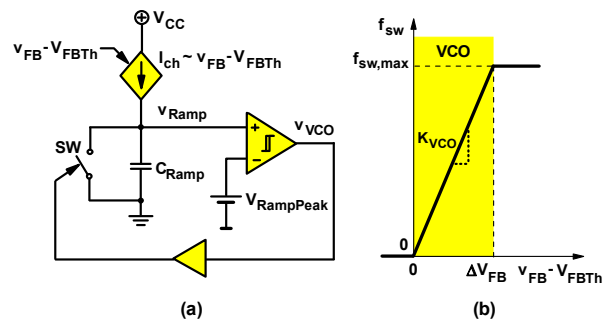

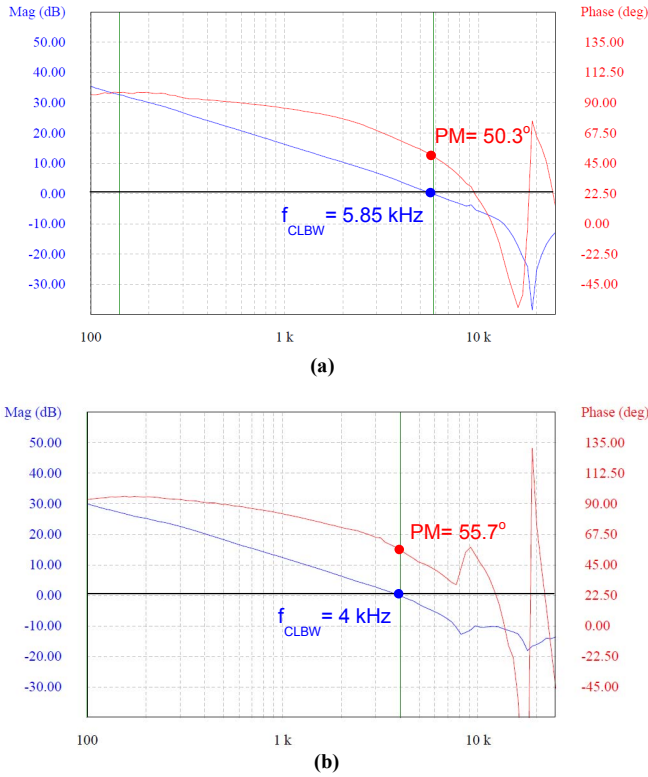Fig. 3 VCO (a) circuit diagram, and (b) transfer function

(a)

(b)

Fig. 4   Closed-loop gain measurements obtained on an 85-W (20.5-V/4.15-A) flyback adapter/charger in DCM operating in FFM at V_{IN}=125V and (a) 10% load, (b) 5% load

(a)

(b)

Fig. 5   Closed-loop gain simulations in SIMPLIS obtained on an 85-W (20.5-V/4.15-A) flyback adapter/charger in DCM operating in FFM at V_{IN}=125V and (a) 10% load, (b) 5% load

For proper design of the feedback circuit, an accurate small-signal model of the flyback converter with variable switching frequency in both DCM/CCM boundary and DCM operating in FFM is necessary.   The conventional averaged small-signal model of the variable switching frequency flyback converter [3] provides results which are in good agreement with the experimental results as long as the switching frequency is well above the closed-loop bandwidth.   However, as the switching frequency of DCM flyback converter operating in the FFM decreases with the load and approaches the bandwidth frequency, measurements show that the bandwidth frequency also starts decreasing.   Closed-loop gain measurements obtained on an 85-W (20.5-V/4.15-A) flyback adapter/charger in DCM operating in FFM are presented in Fig. 4.   As shown in Fig. 4, at 10% load (where $f_{sw} \approx 18.4$ kHz), the closed-loop bandwidth is $f_{CLBW} = 5.85$ kHz, whereas, at 5% load (where $f_{sw} \approx 9$ kHz), the closed-loop bandwidth is reduced to 4 kHz.   Similar results can be obtained by simulations.   For example, closed-loop gain simulations obtained in SIMPLIS are shown in Fig. 5.   As can be seen, the simulation results are in close agreement with the experimental results.   However, according to the conventional averaged small-signal model of the DCM flyback operating in the FFM, the closed-loop bandwidth does not change when the switching frequency decreases with the load.

In this paper, the discrepancy between the averaged small-signal model and measurements is investigated.   It is found that the source   of this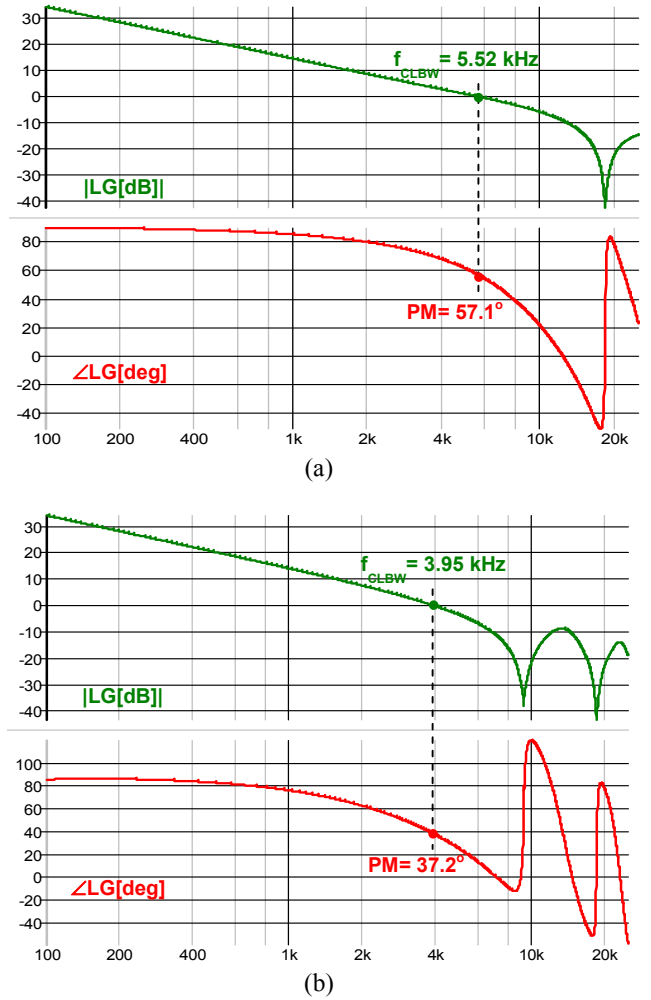 discrepancy   is the   nonlinearity   of the voltage controlled oscillator.   In fact, the VCO generates sideband frequency components [4]-[7] similar to the conventional pulse width modulator (PWM) [4], [5], [8]-[11].   By including the effect of the sideband components in the closed loop, a multi-frequency averaged small-signal model of the DCM flyback converter in the FFM is proposed.

II.   AVERAGED SMALL-SIGNAL MODEL OF DCM FLYBACK CONVERTER IN FFM OF OPERATION

Key waveforms of the DCM flyback converter operating in FFM are shown in Fig. 6, where L_M and N denote the magnetizing inductance and the turns ratio N_P/N_S of the flyback transformer.   The average diode current over a switching period $T_{sw} = 1/f_{sw}$, which is equal to the load current I_O, can be determined as

$$i_{Dav} = \langle i_D \rangle_{T_{sw}} = \frac{L_M}{2 R_{CS}^2} \cdot \frac{V_{CS,REF}^2}{V_O} \cdot f_{sw} = f(f_{sw}, V_O) \quad . \quad (1)$$
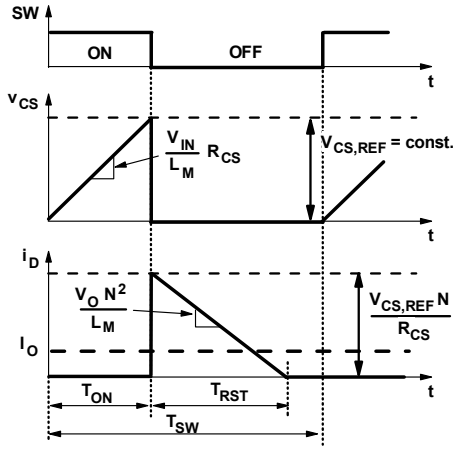
Fig. 6   Key waveform of DCM flyback converter in FFM

As shown in (1), if $V_{CS,REF}$ is constant, the switching frequency is proportional to the load current. Then, the small-signal variation of the diode current is obtained as

$$\hat{i}_{Dav} = k_{sw} \cdot \hat{f}_{sw} - \frac{1}{r_O} \cdot \hat{v}_O \quad , \qquad (2)$$

where,

$$k_{sw} = \frac{L_M}{2R_{CS}^2} \cdot \frac{V_{CS,REF}^2}{V_O} \quad , \qquad (3)$$

and

$$\frac{1}{r_O} = \frac{L_M}{2R_{CS}^2} \cdot \frac{V_{CS,REF}^2}{V_O^2} \cdot f_{sw} = \frac{I_O}{V_O} = \frac{1}{R_L} \quad . \qquad (4)$$

Assuming a linear VCO transfer function as that shown in Fig. 3(b), the relationship between small-signal frequency change $\hat{f}_{sw}$ and small-signal change of feedback voltage $\hat{v}_{FB}$ is given by

$$\hat{f}_{sw} = K_{VCO} \cdot \hat{v}_{FB} \quad . \qquad (5)$$

Based on (2)-(5), the conventional averaged small-signal model of the DCM flyback in the FFM is obtained as shown in Fig. 7, which can be simplified as shown in Fig. 8, where

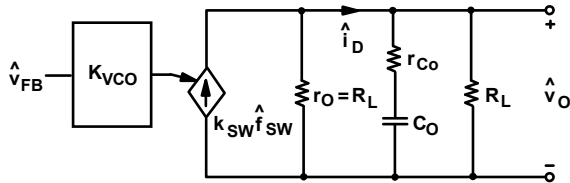$$g_{FB} = K_{VCO} \cdot k_{sw} \quad . \qquad (6)$$

Fig. 7   Conventional averaged small-signal model of DCM flyback converter in FFM
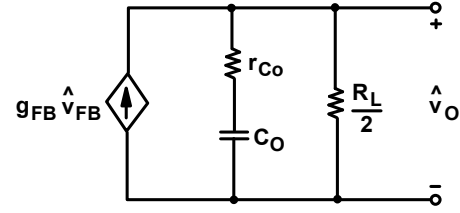

Fig. 8   Simplified conventional averaged small-signal model of DCM flyback converter in FFM

The asymptotic Bode plots of the control-to-output transfer function

$$G_{vc}(j\omega) = \frac{\hat{v}_O}{\hat{v}_{FB}} = K_{vc} \cdot \frac{1 + j\omega/\omega_z}{1 + j\omega/\omega_p} \quad . \qquad (7)$$

where,

$$K_{vc} = g_{FB} \cdot \frac{R_L}{2} \quad , \qquad (8)$$

$$\omega_z = \frac{1}{r_{Co} C_O} \quad , \qquad (9)$$

and

$$\omega_p = \frac{1}{(r_{Co} + R_L/2)C_O} \approx \frac{2}{R_L C_O} \quad , \qquad (10)$$

are presented in Fig. 9.

As it can be seen in Fig. 9, only the low-frequency part of the control-to-output transfer function changes with the load. Since the closed-loop bandwidth is typically located inside the frequency range highlighted in green in Fig. 9 and since the transfer function of the feedback circuit is independent of the load, it can be concluded that the closed-loop bandwidth does not change with the load.
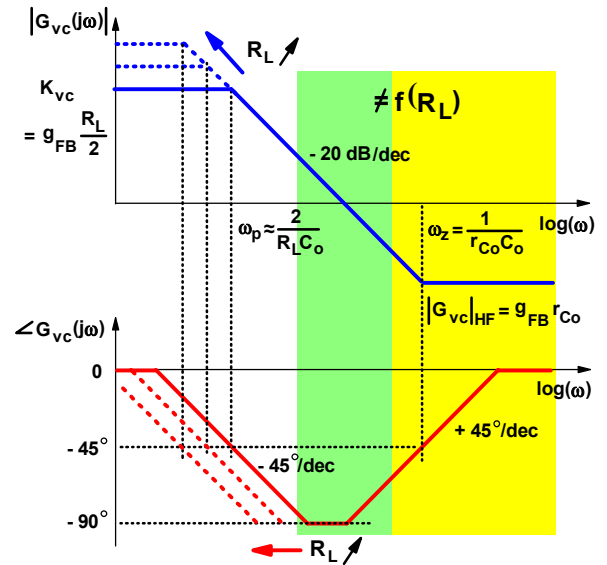

Fig. 9   Asymptotic Bode plots of control-to-output transfer function of DCM flyback converter in FFM
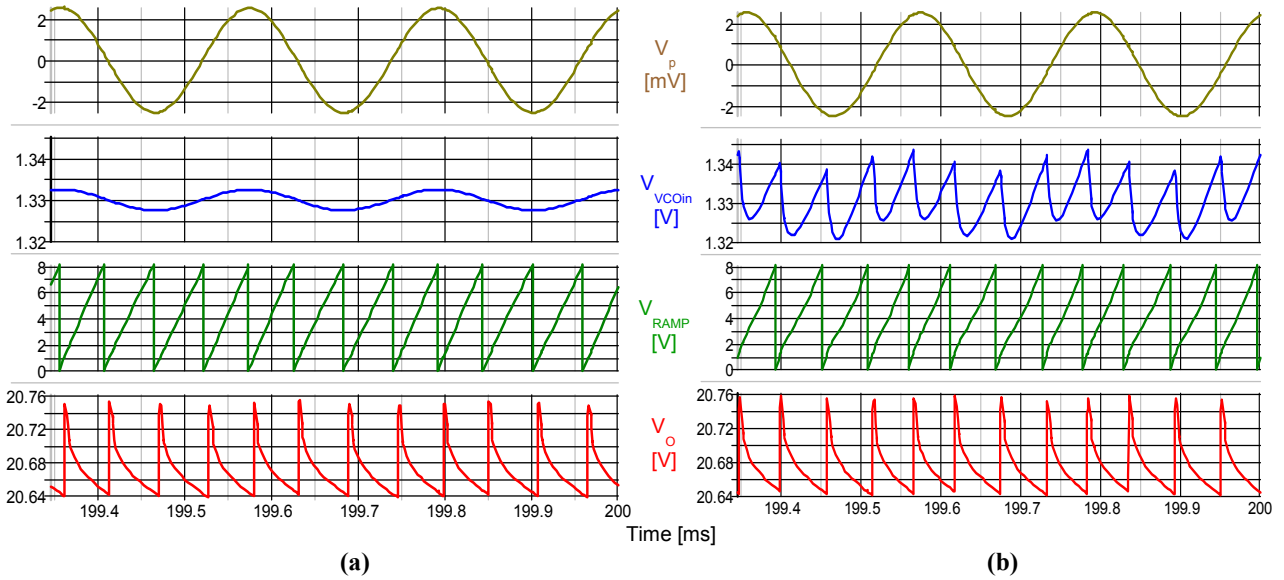
Fig. 10   Simulation waveforms of DCM flyback in FFM at V_{IN} = 125 V, at 10% load, with sinusoidal perturbation frequency $f_p = f_{sw}/4$ = 4.6 kHz in (a) open loop and (b) closed loop
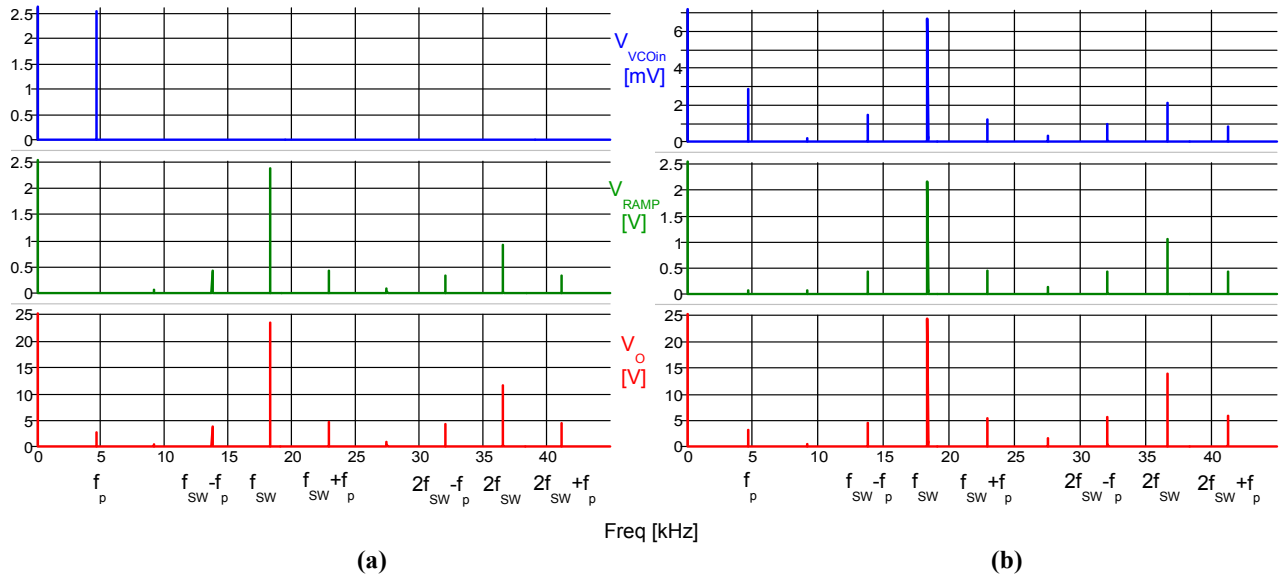

Fig. 11   Simulation spectra of DCM flyback in FFM at V_{IN} = 125 V, at 10% load, with sinusoidal perturbation frequency $f_p = f_{sw}/4$ = 4.6 kHz in (a) open loop and (b) closed loop

III.   EFFECT OF SIDEBAND FREQUENCY COMPONENTS

Closed-loop measurements of the DCM flyback in FFM are in disagreement with the conventional averaged small-signal model. In fact, as the switching frequency decreases with decreasing load, the closed-loop bandwidth also decreases, as shown in Fig. 4. To understand the discrepancy between the conventional averaged small-signal model and measurements, the DCM flyback in FFM is simulated in SIMPLIS. An

85-W (20.5-V/4.15-A) dc/dc flyback converter was used as the example circuit. In Fig. 2,

$$v_p = V_{pm}\cos(2\pi f_p t + \theta_p) \quad . \qquad (11)$$

is the perturbation voltage source. Both, open-loop (OL) and closed-loop (CL) simulations were performed.

In Figs. 10 and 11, relevant simulation waveforms and corresponding spectra, obtained at 10% load (where the

1749

switching frequency is f_{sw} = 18.4 kHz) with a sinusoidal perturbation frequency $f_p = f_{sw}/4 = 4.6$ kHz, illustrate the differences between operations in open loop and closed loop. In open-loop, as shown in Fig. 11(a), at the input of the VCO, there are only two components: the dc component, which determines the steady-state switching frequency, and the perturbation frequency component. The spectrum of the VCO ramp voltage consists of a dc component, the switching frequency component and its harmonics, the perturbation frequency component and, in addition, sideband frequency components $f_{sw} \pm f_p$, $2f_{sw} \pm f_p$, etc. This means that the VCO is a nonlinear circuit, similar to the conventional pulse width modulator (PWM) [4], [5], [8]-[11]. All the frequency components at the output of the VCO appear in the spectrum of the output voltage. In closed loop, as shown in Fig. 11(b), at the input of the VCO, besides the dc component and the perturbation frequency component, there are all the other frequency components present in the output voltage. Consequently, the spectrum of the VCO ramp voltage and, furthermore, the spectrum of the output voltage in closed loop differ from the corresponding spectra in open loop. This difference is the result of the nonlinearity of the VCO and can be explained by considering the lowest sideband component $f_{sw} - f_p$ and its effect on the closed loop as illustrated in Figs. 12 and 13. If the perturbation frequency is small such that $f_p \ll f_{sw}$, then $f_{sw} - f_p$ is close to f_{sw} and above the closed-loop bandwidth f_{CLBW}. Therefore, sideband component $f_{sw} - f_p$ will be attenuated before fed back through the feedback circuit to the VCO input and its effect on the loop gain is negligible. However, if f_p is close to f_{sw} such that $f_{sw} - f_p < f_{CLBW}$, then $f_{sw} - f_p$ will be amplified before fed back to the VCO input and its effect on the loop gain is not negligible. It is shown in Section IV that the loop gain is decreased around the switching frequency, which results in a decrease of the closed-loop bandwidth.
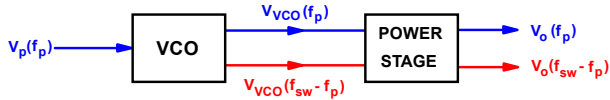

Fig. 12   Frequency domain representation of open-loop DCM flyback in FFM with sideband components
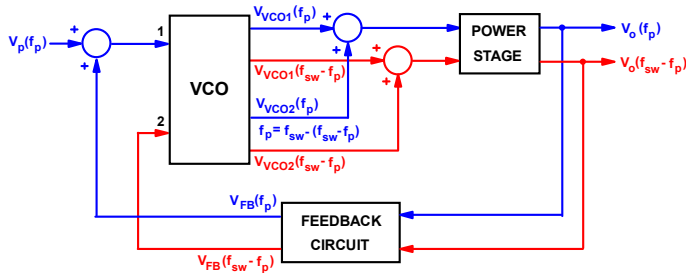

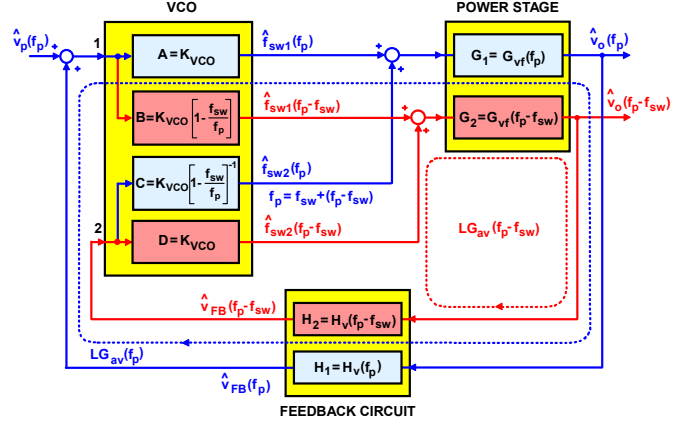Fig. 13   Effect of sideband components in closed-loop DCM flyback in FFM

Fig. 14   Multi-frequency averaged small-signal model of DCM flyback converter in FFM

IV. MULTI-FREQUENCY AVERAGED SMALL-SIGNAL MODEL OF DCM FLYBACK CONVERTER IN FFM OF OPERATION

The spectrum of the frequency modulated pulses at the output of the VCO was derived in [4] and [6] as

$$v_{VCO}(t) = AV_{FBdc}K_{VCO} + AV_{pm}K_{VCO}\cos(2\pi f_p t + \theta_p) +$$
$$2A\sum_{k=1}^{\infty}\sum_{n=-\infty}^{\infty}J_n\left(\frac{kV_{pm}K_{VCO}}{f_p}\right)\cdot\frac{kf_{sw}+nf_p}{k}\cdot \qquad ,(12)$$
$$\cos\left[2\pi(kf_{sw}+nf_p)t+n\theta_p-\frac{kV_{pm}K_{VCO}}{f_p}\cdot\sin\theta_p\right]$$

where, A is the area of the narrow pulses and J_n is the Bessel function of the first kind of order n. In accordance with Figs. 12 and 13, considering only the lowest sideband component $f_{sw} - f_p$, (12) can be simplified as

$$v_{VCO}(t) = AV_{FBdc}K_{VCO} + AV_{pm}K_{VCO}\cos(2\pi f_p t + \theta_p) +$$
$$2AJ_{-1}\left(\frac{V_{pm}K_{VCO}}{f_p}\right)\cdot(f_{sw}-f_p)\cdot \qquad .(13)$$
$$\cos\left[2\pi(f_{sw}-f_p)t-\theta_p-\frac{V_{pm}K_{VCO}}{f_p}\cdot\sin\theta_p\right]$$

In small-signal analysis, it can be assumed that the perturbation amplitude V_{pm} is very small and, therefore, (13) can be further simplified as

$$v_{VCO}(t) = AV_{FBdc}K_{VCO} + AV_{pm}K_{VCO}\cos(2\pi f_p t + \theta_p) -$$
$$- A\frac{V_{pm}K_{VCO}}{f_p}\cdot(f_{sw}-f_p)\cdot\cos\left[2\pi(f_{sw}-f_p)t-\theta_p\right] \qquad ,(14)$$

where the Bessel function J_{-1} is approximated as

$$J_{-1}(x) \approx -\frac{x}{2} \quad \text{when} \quad x \ll 1 \ . \qquad (15)$$

It should be noted in (14) that the sideband frequency component f_{sw}-f_p at the VCO output has inverted sign of initial phase angle θ_p. In order to avoid more complex mathematical expressions, it is convenient to consider the negative sideband frequency component f_p-f_{sw} instead of the positive sideband frequency component f_{sw}-f_p [10]. Then, (14) can be rewritten as

$$v_{VCO}(t) = AV_{FBdc}K_{VCO} + AV_{pm}K_{VCO}\cos(2\pi f_p t + \theta_p) -$$
$$- A\frac{V_{pm}K_{VCO}}{f_p}\cdot(f_{sw}-f_p)\cdot\cos\left[2\pi(f_p-f_{sw})t+\theta_p\right] \quad ,(16)$$

Combining (16) and the block diagram in Fig. 13, the multi-frequency averaged small-signal (MFASS) model of the DCM flyback in FFM can be obtained as shown in Fig. 14, where $G_{vf}(f) = \hat{v}_O/\hat{f}_{sw}$ and $H_v(f) = \hat{v}_{FB}/\hat{v}_O$ are the transfer functions of the power stage and the feedback circuit, respectively.

The closed-loop gain at the perturbation frequency is obtained as

$$LG(f_p) = \frac{AG_1H_1+(BC-AD)G_1H_1G_2H_2}{1-DG_2H_2} \quad . \quad (17)$$

Since,

$$BC = AD = K_{VCO}^2 \quad , \quad (18)$$

the closed-loop gain (17) is determined as

$$LG(f_p) = \frac{AG_1H_1}{1-DG_2H_2} \quad . \quad (19)$$

Finally, the closed-loop gain (19) can be rewritten as

$$LG(f_p) = \frac{K_{VCO}\cdot G_{vf}(f_p)\cdot H_v(f_p)}{1-K_{VCO}\cdot G_{vf}(f_p-f_{sw})\cdot H_{vf}(f_p-f_{sw})} = \frac{LG_{av}(f_p)}{1-LG_{av}(f_p-f_{sw})}$$

(20)

where LG_{av} is the closed-loop gain of the conventional averaged small-signal model.

Comparison of the closed-loop gains of the DCM flyback in FFM obtained with the conventional averaged small-signal model and with the MFASS model is presented in Fig. 15. The closed-loop gain obtained with the MFASS model is in a good agreement with the corresponding closed-loop gain obtained with measurements. As can be seen in Figs. 4 and 15, the closed-loop bandwidth of the DCM flyback in FFM decreases by approximately 1.9 kHz when the load decreases from 10% to 5%.

V. SUMMARY

The conventional averaged small-signal model of the DCM flyback converter in the FFM of operation shows that the closed-loop bandwidth does not change with the load. However, this is not in agreement with the closed-loop measurements. In this paper, the discrepancy between the conventional averaged small-signal model and measurements is investigated. It is found that the source of this discrepancy is the
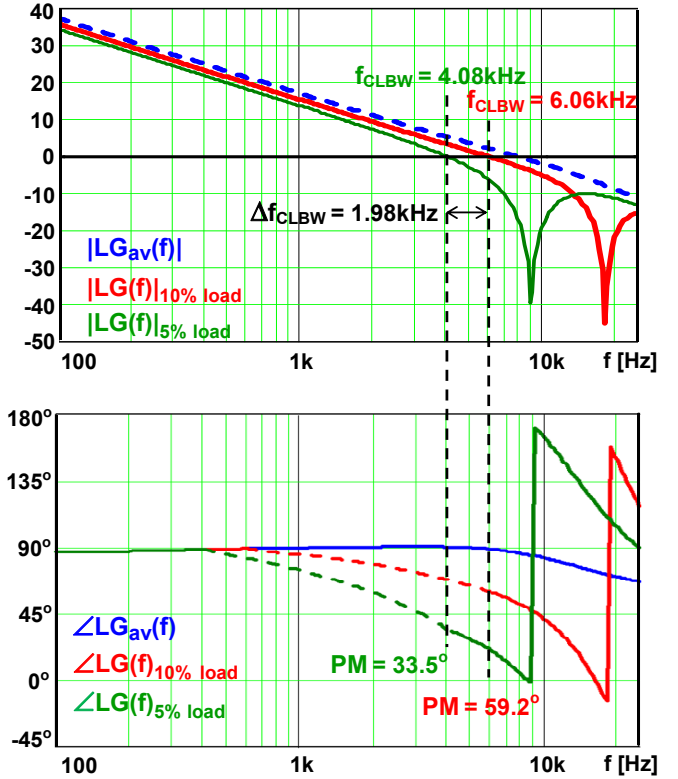

Fig. 15 Closed-loop gain of DCM flyback in FFM [85-W (20.5-V/4.15-A)] obtained with conventional averaged small-signal model (blue line); and with multi-frequency averaged small-signal model at 10% load, where f_{SW} = 18.4 kHz, (red line), and 5% load, where f_{SW} = 9 kHz, (green line), at V_{IN}=125V

voltage controlled oscillator. In the conventional averaged small-signal model, the VCO is represented with a linear relationship $f_{sw} = K_{VCO}\cdot v_{VCOin}$. However, the VCO is a nonlinear circuit and it generates sideband frequency components similar to the conventional pulse width modulator (PWM) [4], [5], [8]-[11]. The effect of the nonlinearity of the VCO on the closed-loop is explained by considering the case when f_{sw} is not significantly greater than the closed-loop bandwidth f_{CLBW} and by considering the lowest sideband component f_{sw}-f_p. If the perturbation frequency f_p is small such that $f_p \ll f_{sw}$, then f_{sw}-f_p is close to f_{sw} and above f_{CLBW}. Therefore, sideband component f_{sw}-f_p will be attenuated before fed back through the feedback circuit to the VCO input and its effect on the loop gain is negligible. However, if f_p is close to f_{sw} such that f_{sw}-$f_p < f_{CLBW}$, then f_{sw}-f_p will be amplified before fed back to the VCO input and its effect on the loop gain is not negligible. Including the effect of the sideband components in the closed loop, a multi-frequency averaged small-signal (MFASS) model of the DCM flyback in FFM is proposed. The closed-loop gain obtained with the MFASS model is in a good agreement with the corresponding closed-loop gain obtained with measurements.

REFERENCES

[1] Environmental Protection Agency (EPA), "Energy Star Program requirements for single voltage external ac-dc and ac-ac power supplies," available at http://www.energystar.gov/ia/partners/product_specs/program_reqs/EPS%20Eligibility%20Criteria.pdf

[2] European Commission, "Code of Conduct on energy efficiency of external power supplies," available at http://sunbird.jrc.it/energyefficiency/pdf/Workshop_Nov.2004/PS%20meeting/Code%20of%20Conduct%20for%20PS%20Version%202%2024%20November%202004.pdf

[3] B.T. Irving, Y. Panov, and M.M. Jovanović, "Small-signal model of variable-frequency flyback converter," *Proc. Applied Power Electronics Conf. (APEC)*, pp. 977-982, Feb. 2003.

[4] E. Fitch, "The spectrum of modulated pulses," *Journal IEE*, vol. 94, part 3A, pp. 556-564, 1947.

[5] P. F. Panter, *Modulation, noise, and spectral analysis applied to information transmission*. New York, NY: McGraw Hill, 1965.

[6] E.J. Bayly, "Spectral analysis of pulse frequency modulation in the nervous systems," *IEEE Trans. Bio-Medical Engineering*, vol. BME-15, no 4, pp. 257-265, Oct. 1968.

[7] Y. Huang and J. Sun, "Spectrum of pulse frequency modulation," *Journal on Semiconductor, Photonics, and Technology*, vol. 2, no. 3, pp. 194-198, Aug. 1996.

[8] R.D. Middlebrook, "Predicting modulator phase lag in PWM converter feedback loops," *Proc. Intn'l Solid-State Power Electronics Conf. (Powercon)*, pp. 245-250, Apr. 1981.

[9] Z. Song and D.V. Sarwate, "The frequency spectrum of pulse width modulated signals," *Intn'l Journal on Signal Processing*, Elsevier B.V., vol. 83, issue 10, pp. 2227-2258, Oct. 2003.

[10] Y. Qiu, M. Xu, K. Yao, J. Sun, and F.C. Lee, "Multifrequency small-signal model for buck and multiphase buck converters," *IEEE Trans. Power Electronics*, vol. 21, no 5, pp. 1185-1192, Sep. 2006.

[11] H.T. Mouton and B. Putzeys, "Understanding the PWM nonlinearity: single-sided modulation," *IEEE Trans. Power Electronics*, vol. 27, no 4, pp. 2116-2128, Apr. 2012.